J. Plasma Physics (2001), *vol.* 65, *part* 1, *pp.* 59–72. Printed in the United Kingdom

The ignition brachystochrone

A. SESTERO

Associazione EURATOM–ENEA sulla Fusione, Centro Ricerche Frascati, CP 65, 00044 Frascati (RM), Italia

(Received 27 March 2000 and in revised form 3 July 2000)

Abstract. The path is sought in the temperature–density plane that allows desired plasma burning conditions to be reached in the shortest possible time. This task is undertaken using the tools of classical variational analysis. The derived expression of Euler's equation is found to be degenerate. Ways to overcome such an impasse are examined, and eventually the solution is obtained. Illustrative applications to the OMITRON proposed ignition experiment are presented, which make reference to the Lackner–Gottardi and ITER-P89 scalings for the energy confinement time.

1. Introduction

The present paper is targeted specifically at the *non-superconducting ignition experiments* that are currently being proposed by a number of fusion laboratories. Indeed, it is well recognized that in a non-superconducting ignition experiment, the need to reach plasma burning conditions within the allowed pulse length (as determined, typically, by the Joule heating of the toroidal magnet) imposes an important constraint. This means that one is actually not allowed to waste any time in steering the plasma toward ignition – implying that one must take advantage of strategies properly optimized to that end.

For some of the device parameters and plasma parameters that are involved, the strategies to follow are actually obvious: for example, the induced plasma current must be at all times as large as permitted by the involved constraints, the impurity content must be at all times as low as possible, etc. For one plasma parameter in particular, however – the plasma density – the optimization prescription is not that obvious. The scope of the present paper is indeed to find out which density control pattern is required to drive the plasma to ignition within the shortest possible time.

In this paper the key features characterizing the problem are examined, and illustrated with the help of a simplified, zero-dimensional, pilot calculation. In the latter, for the sake of simplicity, all considered device and plasma parameters – with the important exceptions of plasma *temperature* and plasma *density* – are held constant with respect to time. The problem thus reduces to finding the trajectory in the *temperature–density* plane that minimizes the time needed to reach plasma burning conditions. This is in a way reminiscent of the search for the *brachystochrone* – a famous problem going back to the early days of rational mechanics and the calculus of variations. In analogy, therefore, we have chosen here to refer to our sought-after optimal path in the temperature–density plane as the 'ignition brachystochrone'.

2. The unconstrained extremal problem

Our calculation proceeds from the obvious relation

$$\frac{dE}{dt} = P, \tag{1}$$

where E is the total kinetic energy content of the plasma, P is the net power input into the plasma, and t is the time. The plasma kinetic energy E can be expressed as

$$E = NW, \tag{2}$$

where N is the total number of particles (electrons, fuel ions, and impurity ions) in the plasma, and W is the mean kinetic energy *per* plasma particle. The quantities N and W can in turn be written as

$$N = 2VC\bar{n}, \qquad W = \frac{3}{2}k\tilde{T}, \tag{3a, b}$$

where $\bar{n}$ is the average *electron* density, V is the plasma volume, C is the coefficient required to properly relate $\bar{n}$ to N in the presence of impurities (see further in Sec. 4), k is Boltzmann's constant, and $\tilde{T}$ is the appropriately defined average of the temperature that is required for (3b) to hold (see again Sec. 4).

From the expression for E thus obtained

$$E = 3VC\bar{n}k\tilde{T}, \tag{4}$$

one can express the total differential dE in terms of the differentials $d\bar{n}$ and $d\tilde{T}$ (remembering that everything else in the problem is taken to be constant):

$$dE = 3VCk(\bar{n}\,d\tilde{T} + \tilde{T}\,d\bar{n}). \tag{5}$$

As the next step, we prescribe a trajectory S in the $(\bar{n}, \tilde{T})$ plane, and require the point representative of our physical system to stay on such a trajectory. The differentials $d\bar{n}$ and $d\tilde{T}$ are thus no longer independent, and we can write

$$dE = 3VCk\left(\bar{n} + \tilde{T}\frac{d\bar{n}}{d\tilde{T}}\right)d\tilde{T}, \tag{6}$$

with the quantity $d\bar{n}/d\tilde{T}$ being defined by the local trajectory slope. A further step – whereby (6) is related back to (1) – produces the following expression for the differential dt of the time variable, calculated along the given trajectory:

$$dt = \frac{dE}{P} = 3VCk\frac{\bar{n} + \tilde{T}\,d\bar{n}/d\tilde{T}}{P(\bar{n}, \tilde{T})}d\tilde{T}, \tag{7}$$

where on the right-hand side, the fact that the net power P is a function of $\bar{n}$ and $\tilde{T}$ has been directly emphasized. Equation (7) clearly enables us to compute the time t_s taken by our physical system to evolve from start to end along the introduced trajectory S:

$$t_s = \int_S F(\tilde{T}, \bar{n}, \bar{n}')\,d\tilde{T}, \tag{8}$$

where

$$F(\tilde{T}, \bar{n}, \bar{n}') = 3VCk\frac{\bar{n} + \tilde{T}\bar{n}'}{P(\tilde{T}, \bar{n})}, \qquad \bar{n}' = \frac{d\bar{n}}{d\tilde{T}}. \tag{9a, b}$$

https://doi.org/10.1017/S0022377801008911 Published online by Cambridge University Press

Having thus properly set the stage, we are in a position to formulate the *extremal problem* in which we are interested. Given, in the $(\bar{n}, \tilde{T})$ plane, a *starting point* (representative of well-established plasma conditions, attained somewhat after discharge breakdown) and an *end point* (representative of the regime of plasma burning at which we are aiming), within the collection of all possible trajectories connecting the two points, we must seek out the one that makes the evolution time t_s (as computed from the integral in (8)) the *shortest*. This problem is typical of the discipline of the calculus of variations, and its solution, as is well known, can be found with the help of *Euler's equation* (here written with reference to the notation of (8)):

$$\frac{\partial^2 F}{\partial \bar{n}'^2}\bar{n}'' + \frac{\partial^2 F}{\partial \bar{n}'\,\partial \bar{n}}\bar{n}' + \frac{\partial^2 F}{\partial \bar{n}'\,\partial \tilde{T}} - \frac{\partial F}{\partial \bar{n}} = 0. \tag{10}$$

Before carrying on with our specific case, it is important to point out that in the vast majority of mechanical and physical applications, the integrand in the expression that is to be extremized is a *nonlinear* function of the first derivative of the unknown (in our notation, that would mean of $\bar{n}'$). Under such circumstances, Euler's equation is a second-order ordinary differential equation for the unknown function (in our notation, that would be the function $\bar{n}(\tilde{T})$). The general solution of a second-order differential equation, obviously, contains two arbitrary constants, which can in principle be fixed by requiring the solution to go through a starting point and an end point conveniently assigned. This pins down the sought-after extremal trajectory uniquely.

On the other hand, however, it so happens that in our problem the integrand $F(\tilde{T}, \bar{n}, \bar{n}')$ depends on $\bar{n}$ only *linearly* (as a glance at (9a) promptly reveals). This circumstance actually entails special consequences. In order to bring the latter to light, let us make this linearity explicit by writing the integrand in the form

$$F(\tilde{T}, \bar{n}, \bar{n}') = G_1(\tilde{T}, \bar{n})\,\bar{n}' + G_2(\tilde{T}, \bar{n}), \tag{11}$$

where

$$G_1(\tilde{T}, \bar{n}) = \frac{3VCk\tilde{T}}{P(\tilde{T}, \bar{n})}, \qquad G_2(\tilde{T}, \bar{n}) = \frac{3VCk\bar{n}}{P(\tilde{T}, \bar{n})}. \tag{12a, b}$$

Upon substituting (11) and (12) into (10), one can appreciate that some important simplifications take place, on account of which Euler's equation comes eventually to be written as follows:

$$\frac{\partial G_1(\tilde{T}, \bar{n})}{\partial \tilde{T}} - \frac{\partial G_2(\tilde{T}, \bar{n})}{\partial \bar{n}} = 0. \tag{13}$$

The feature that is most worth emphasizing in the latter expression is that both the first and second derivatives of the unknown function $\bar{n}(\tilde{T})$ are missing from it: implying, therefore, that Euler's second-order differential equation has degenerated into a zeroth-order, *finite* equation. The latter, clearly, specifies a *unique* curve in the $(\bar{n}, \tilde{T})$ plane, whose role and meaning in the context of the considered extremal problem is a priori not clear. For convenience, in this paper, we shall introduce a special name for this curve: for reasons that will indeed become clear in the sequel, we shall term it the *brachystochrone kernel curve*.

https://doi.org/10.1017/S0022377801008911 Published online by Cambridge University Press

It is important here to emphasize that the reason why the function F displays the linear behaviour expressed by (11) – and hence why Euler's equation becomes degenerate – can be ultimately tracked down to (2): which expresses the basic fact that kinetic energies of single particles combine additively to yield the total kinetic energy content E of the plasma. Thus the degeneracy of Euler's equation is apparently describing a fundamental physical feature of our problem, and we must live with it.

Looking for help on how to deal with such a degeneracy in Euler's equation, we may try browsing through the literature.† By so doing, we may eventually meet the following statement (Elsgolc 1962): if the assigned starting and end points both belong to the curve that is the solution of the degenerate Euler equation then (it is claimed) the arc of this curve between these two points is indeed an extremal trajectory; if, on the other hand, the two assigned points do not both belong to this curve then the formulated variational problem has no solution (i.e. no extremal trajectory exists).

It is perhaps appropriate here to recall that any statement about extremals is a statement about the existence of an extremal *in the small* (that is, in the context of a first-order, perturbative searching procedure). Hence the existence of such an extremal *in the small* does not guarantee that a corresponding extremal exists also *in the large* (that is, in an absolute sense). Indeed, as an addendum to the above-quoted statement from the literature, it can be proved that – as far as our case is concerned – a minimum *in the large* of the time t_s *never* exists, even if the starting and end points are both assigned to belong to the brachystochrone kernel curve.

The above statements appear at first rather puzzling. Physical intuition would in fact seem to suggest that in the considered problem an extremal trajectory ought to exist for any arbitrarily assigned starting and end points in the $(\bar{n}, \tilde{T})$ plane. A way out of this dilemma can perhaps be found in the considerations that follow. It may be, indeed, that there is a flaw in our procedure, to be imputed possibly to the fact that we have been searching for an extremal within an ensemble of trajectories that is *too large*. Not all mathematically allowed trajectories may in fact be physically acceptable. Perhaps, then, if we were to properly trim down the set of trajectories among which to search, we might find, after all, that an extremal trajectory does exist, indeed, for any arbitrarily assigned starting and end points. This obviously suggests that we must look to that area of the calculus of variations that deals with the so-called *constrained extremal problems* (see e.g. Garfinkel 1967). We shall do that in the next section.

3. The constrained extremal problem

To help us get to the root of the problem, let us begin by noting that *everywhere* in the $(\bar{n}, \tilde{T})$ plane, trajectory elements can be constructed that make the time differential dt defined by (7) a *negative* quantity. Readers may themselves easily

† Actually, quite a large number of current books on the calculus of variations make no comment on the possible occurrence of the above-noted degeneracy in Euler's equation. An exception is the didactically oriented book by Elsgolc (1962), where at least the reader is presented with the statement about the issue that we are reporting above.

https://doi.org/10.1017/S0022377801008911 Published online by Cambridge University Press

ascertain the truth of this statement.† Now, by assembling many such trajectory elements together, trajectories can clearly be constructed that are characterized by arbitrarily large *negative* transit times. This explains why a minimum transit time does not exist, in general, for trajectories starting and ending at arbitrarily assigned pairs of points in the $(\bar{n}, \tilde{T})$ plane.

However, trajectory elements yielding negative values of dt have no physical meaning, since the time parameter t, obviously, can only grow along any physically admissible trajectory. We are thus led, sensibly, to place the constraint $dt \geqslant 0$ on all elemental arcs of our sought-after extremal curve. Such a constraint clearly specifies the value 0 to be a lower bound for the transit time of *any* trajectory: implying therefore that minimum-time trajectories do indeed exist in this case for any assigned starting and end points.

In the case that is of concern to us, however, the condition $dt \geqslant 0$ is possibly still too lenient. Under this condition, indeed, trajectorial arcs are still allowed along which the *density parameter rate of change* (i.e. the quantity $d\bar{n}/dt$) can be very large‡ – possibly larger than, on physical grounds, it can be allowed to be. There are, in fact, obvious physical and/or technological limitations that affect the rate at which $\bar{n}$ can either *grow* or *decrease*. The rate of density growth is controlled typically by fuel feed mechanisms (gas puffing and/or pellet injection), while the rate of density decrease can in some way be understood to be related to particle transport in the plasma. All this suggests that on all trajectory elements that make up our sought-after optimal path, we should perhaps place a pair of *unilateral constraints* of the following type:

$$-\frac{\bar{n}}{\alpha\tau_E} \leqslant \frac{d\bar{n}}{dt} \leqslant \bar{n}_t, \tag{14}$$

where the lower limit on the density rate of change (the left-hand side) is expressed in terms of the *particle confinement* time $\alpha\tau_E$ (written, as is often done, as the energy confinement time τ_E times a multiplicative factor α), while the upper limit (the right-hand side) is simply taken to be a constant value $\bar{n}_t$, selected on the basis of the performance ascribed to the fuel-feed mechanisms employed. Clearly, because of (7) and (9b), (14) can also be rewritten as follows:

$$-\frac{\bar{n}}{\alpha\tau_E} \leqslant \frac{P}{3kV(\bar{n} + \tilde{T}\bar{n}')}\bar{n}' \leqslant \bar{n}_t, \tag{15}$$

where the two constraints must be thought of as being imposed on $\bar{n}'$.

Having thus convinced ourselves that the variational problem that concerns us must be reformulated as a *constrained extremal problem* – so as to indeed include the *unilateral constraints* expressed by (15) in an essential way – we shall here take a little time to recall the main features that characterize *constrained extremal problems* in the calculus of variations. The point that needs to be made is that in the latter framework, extremal trajectories are no longer (in general) fully smooth curves, but are instead typically constructed as sequences of

† It must be remembered, of course, that a trajectory element is identified by specifying an infinitesimal arc *plus* a sense of orientation on it.

‡ As a matter of fact, since the differential dt occurs in the denominator of the expression for the density parameter rate of change, near the limit of the condition $dt \geqslant 0$, the fact that dt can be very small may be understood to imply that the density parameter rate of change can actually become arbitrarily large.

https://doi.org/10.1017/S0022377801008911 Published online by Cambridge University Press

smooth sections that join to each other at *corner points*. Adjacent smooth sections satisfy different (finite or differential) equations, to be chosen among a set that comprises Euler's equation together with the equations obtained by taking the equalities in the unilateral constraints that have been introduced into the problem. Many different forms can be envisioned, in principle, for the resulting composed extremal curves, and to find the correct one, it is very often necessary to rely principally on physical common sense and/or trial-and-error procedures.

Applying all this to our problem, we are led to identify the following type of construction of the brachystochrone as the appropriate one for our case of concern. To begin with, one must calculate the *brachystochrone kernel curve* defined in the previous section, and plot it in the $(\bar{n}, \tilde{T})$ plane. The initial and end points of the sought-after optimal trajectory (such as those conceivably assigned to represent a meaningful scenario of the approach to ignition) are likely to lie, typically, far from the brachystochrone kernel curve (in fact, quite far below it in density values). Hence common sense suggests that a three-piece construction of the brachystochrone may be a sensible first-trial choice, with the centre section of the curve being taken from the brachystochrone kernel curve, while the first section leads to it by way of a density increase, and the last section leads away from it by way of a density decrease.

Such a choice proves to be the correct one for a number of significant selections of the set of simulation parameters. For these cases – by applying the prescriptions of conditioned variational analysis recalled above – the first section of the brachystochrone is thus obtained as a solution of the equation resulting from taking the equality in the *right-hand* constraint of (15) (which implies then that the maximum rate of density increase is applied). Solving this equation for $\bar{n}'$, one obtains

$$\bar{n}' = \frac{3kV\bar{n}}{P/\bar{n}_t - 3kV\tilde{T}}. \tag{16}$$

The latter is a first-order differential equation for the unknown $\bar{n}(\tilde{T})$, whose solution is uniquely determined by requiring it to go through the assigned *starting* point in the $(\bar{n}, \tilde{T})$ plane. Obviously, the curve defined by this solution must be followed until it intersects the brachystochrone kernel curve (at which place, the first corner point is located).

To follow, the second section of the brachystochrone must unfold along the brachystochrone kernel curve: that is, along the curve defined by the (finite) equation (13). Note that the latter equation, on account of (12), can also be cast into the simpler form

$$\left(\bar{n}\frac{\partial}{\partial \bar{n}} - \tilde{T}\frac{\partial}{\partial \tilde{T}}\right) P(\tilde{T}, \bar{n}) = 0. \tag{17}$$

Here an important warning is in order, however. In principle, this second section of the brachystochrone can have subsections in which the density is growing and subsections in which it is decreasing. For consistency, it must be checked, obviously, that the constraint on the density increase rate is not violated in the first case, and that the constraint on the density decrease rate is not violated in the second case. If any such violation should indeed occur then a different recipe would have to be applied to the construction of the

https://doi.org/10.1017/S0022377801008911 Published online by Cambridge University Press

brachystochrone: perhaps a four-piece or five-piece construction, instead of the three-piece construction that is being considered here. As an illustration of these concepts, a case with a four-piece construction of the brachystochrone will be presented in Sec. 5.

Finally, the third (and last) section of the extremal curve must be related to the assumed maximum rate of density decrease; that is, it must satisfy the equation obtained by taking the equality in the *left-hand* constraint of (15). Solving this equation for $\bar{n}'$, one obtains

$$\bar{n}' = -\frac{3kV\bar{n}}{P\alpha\tau_E/\bar{n} + 3kV\tilde{T}}. \tag{18}$$

The latter is a first-order differential equation for the unknown $\bar{n}(\tilde{T})$, whose solution is uniquely determined by requiring it to go through the assigned *end* point in the $(\bar{n}, \tilde{T})$ plane. The curve defined by this solution must be followed back, clearly, until it intersects the brachystochrone kernel curve (at which place the second corner point is located).

What has been said so far fully specifies all that is needed for constructing the *ignition brachystochrone* (i.e. our sought-after extremal trajectory). A number of aspects of the discussion here will become clearer in Sec. 5, where the results of some simulations are presented.

4. Plasma simulation model

Before presenting actual simulation results, it is fitting to say a few words to illustrate some key aspects of the computational model adopted. To begin with, we note that in the performed simulations, reference is made to the proposed high-field tokamak ignition experiment known as OMITRON (Barberis et al 1993; for a more complete discussion, see also Sestero 1997). The corresponding values of device and plasma parameters (at least those that are relevant to our problem) are listed in Table 1.† Note that – in complying with the simplifications of the calculation discussed in Sec. 2 – all the quantities listed in Table 1 have been held *constant* with respect to time throughout the performed simulations.

As far as the plasma composition is concerned, the dominant impurity species is assumed to be carbon (originating from the graphite coating of the vessel inner wall). The presence of impurity ions affects various features in the simulation: for the sake of brevity, we omit much of the details here. We feel the need to write down at least one formula, however, which relates the coefficient C in (3a) to the quantities Z_i and f_i listed in Table 1:

$$C = \frac{1}{2}\frac{(Z_i - 1)f_i + 2}{(Z_i - 1)f_i + 1}. \tag{19}$$

At various points in the simulation scheme, integrations over the plasma cross-section are carried out. This requires that information on radial

† It is interesting to compare the OMITRON device parameters with those of the better known IGNITOR proposed experiment: while the dimensions and shape of the plasma doughnut are similar in the two machines, the toroidal field in OMITRON has a much greater strength (due to substantial differences in the toroidal magnet engineering design).

https://doi.org/10.1017/S0022377801008911 Published online by Cambridge University Press

Table 1. Key parameters of simulation model.

Device parameters	
Major radius	1.50 m
Minor radius	0.42 m
Elongation	2.00
Toroidal field on axis	20 T
Toroidal plasma current	15 MA
Additional heating power[a]	24 MW
Plasma parameters (*symbols are defined and/or referred to in Secs* 3 *and* 4)	
Atomic number of dominant impurity, Z_i	6
Fractional abundance of impurity ions,[b] f_i	0.007
Density profile exponent, p_n	1
Temperature profile exponent, p_T	1
Maximum density increase rate, $\overline{n}_t$	5×10^{20} m^{-3} s^{-1}
Particle confinement parameter, α	5

[a] The original design value (see Sestero 1997) was 18 MW. However, recent developments in the design of ICRH launching apparatus for compact high-field tokamak experiments make the increased value adopted here a plausible option.

[b] Defined as the ratio of the number of impurity ions to the total number of ions. The corresponding value of $Z_{\text{effective}}$ is 1.2.

profiles be available: in particular on the radial profiles of the (electron) density n and of the (common) temperature T. In the performed calculations, the radial density and temperature profiles have been actually taken to be of the following forms

$$n \propto \left(\frac{x^2}{a^2}+\frac{y^2}{b^2}\right)^{p_n}, \qquad T \propto \left(\frac{x^2}{a^2}+\frac{y^2}{b^2}\right)^{p_T}. \tag{20a, b}$$

Here the meaning of the symbols is as follows. The plasma cross-section is assumed to have a vertically elongated, elliptical shape, with minor radius a (horizontal) and major radius b (vertical). In the plane of the cross-section, Cartesian coordinates x (horizontal) and y (vertical) are introduced, referred to the plasma centre.

Manifestly, the profiles described by (20) are peaked at the plasma centre, with the degree of peakedness being controlled by the exponents p_n and p_T. Moreover, the profile shapes expressed by (20) have an especially useful property, which can in principle significantly lessen the calculational effort required by the simulation: namely, all integrations over plasma cross-section for which the integrands can be expressed as *polynomials in n and T* can be performed in closed *analytical form*. As a matter of fact, in order to fully exploit the above feature, we took care that all of our integrand functions were indeed written in polynomial form (resorting to suitable polynomial approximations, valid in the correspondingly appropriate ranges of values, for those integrand functions that were not of that form to begin with).‡.

One such cross-sectional integration is required, clearly to produce the

‡ The payoff secured has certainly been non-trivial, if one considers how demanding it would have been, alternatively, to reliably calculate the derivatives appearing in Euler's equation (although only first-order derivatives are present in the degenerate case – see (13)) through an entirely numerical approach.

https://doi.org/10.1017/S0022377801008911 Published online by Cambridge University Press

average electron density $\bar{n}$ used throughout the present paper. Another such integration, similarly, is involved in the derivation of the other key variable used throughout the simulation scheme, namely the quantity $\tilde{T}$. The latter is defined by the relation

$$\tilde{T} = \frac{\overline{nT}}{\bar{n}}, \tag{21}$$

the overbar denoting cross-sectional averaging. On account of the last equation, it is not difficult to show that $\tilde{T}$ is actually a measure of mean energy *per particle*.

As with most other simulation parameters, the profile exponents p_n and p_T have been held constant with respect to time. It should be noted, however, that by so doing one is actually performing calculations that lean significantly towards the pessimistic side: in fact, one is thereby precluding the possibility of exploiting such favourable features as the decoupling of current and temperature profiles in the initial phase, and the peaking of the temperature profile (due to *local ignition*) in the final phase. This ought to be borne in mind when comparing our simple simulation code with other calculational procedures not bound by the same profile-constancy constraint (in particular, that is, with one-dimensional simulation codes, whereby profiles are calculated by solving an appropriate set of diffusion equations).

We come next to discuss the *net power* P, which – of the variables that have been introduced in Sec. 2 – is actually the one that contains the most physical information. In our simulation, the net power P is expressed as the (algebraic) sum of five terms: three *gain terms* (Ohmic power, additional heating power, and α-particle power) and two *loss terms* (radiative Bremsstrahlung power and diffusive transport power). Bulk losses from synchrotron radiation, line radiation, and charge exchange are neglected (a sensible approximation, actually, in view of the high densities that characterize the simulated device). No energy gain is attributed to particles fed into the plasma (their entering energy is low, indeed, compared with the mean energy of plasma particles). Similarly, no energy loss is attributed to particles leaving the plasma (their energy, too, is low compared with the mean energy of plasma particles, because they can only leave after diffusing (and cooling down in the process) from the hot centre region to the cold border plasma).

Of the five terms that we have included in the expression for the net power P, the *additional heating power* is simply prescribed to take on a given constant value throughout the simulation. As for the other terms, three of them (*Ohmic power*, *α-particle power and Bremsstrahlung power*) involve integrations over the plasma cross-section of quantities that are physically well known, and for which reliable expressions – as functions of the local values of density and temperature – are available from the literature. Hence we shall not dwell on these subjects any further here.

Finally, there is the *diffusive-transport power loss*. Of all the terms appearing in the power balance, this is the one that is subject to the greatest uncertainty, as is well known. In our simulations – for lack of better information – we have chosen to model it by two among the most commonly exploited scaling laws for the energy confinement time. For constructing our first example (to be illustrated in Sec. 5) we have chosen the so-called *Lackner–Gottardi scaling*. This scaling has a theoretical basis and some experimental support; moreover, it has

https://doi.org/10.1017/S0022377801008911 Published online by Cambridge University Press

been frequently used† in attempts to predict plasma performance in studies of proposed high-field tokamak ignition experiments such as IGNITOR and OMITRON. Results from an alternative example based on the so-called *ITER-P89 scaling*, will also be presented in Sec. 5. Both of these examples are representative of the family of scalings that embody confinement degradation features.

5. Illustrative examples

For our first example, with *Lackner–Gottardi scaling*, the main results of the performed simulation are depicted in Fig. 1, which shows a portion of the ($\bar{n}$, $\tilde{T}$) plane, with white areas representing domains where the net power P entering the plasma is positive, and shaded areas domains where it is negative. The gap between the *Bremsstrahlung barrier* at the upper left and the *diffusion barrier* at the lower right is sometimes referred to as the *Cordey pass*. Any trajectory leading the plasma system from a point representative of initial plasma conditions on the lower left to a point representative of plasma burning conditions on the upper right must obviously go through this gap.

The partly dashed, partly solid, parabola-like curve that appears to surround the Bremsstrahlung barrier is the *brachystochrone kernel curve*, introduced and discussed in Secs 2 and 3. It must be noted that a *saddle point* of the function $P(\bar{n}, \tilde{T})$ ideally marks the centre of the 'Cordey pass'. Recalling that the saddle point is defined by the simultaneous satisfaction of the two conditions:

$$\frac{\partial P}{\partial \tilde{T}} = 0, \qquad \frac{\partial P}{\partial \bar{n}} = 0, \tag{22a, b}$$

it is an easy step to show that if (22) hold then obviously also (17) is satisfied. In other words, the saddle point itself belongs to the brachystochrone kernel curve.‡

The dashed curve on the upper right of the figure is the locus of points where, *upon switching off the additional heating power*, the system is in thermal equilibrium. More precisely, points lying on the curve to the left of its vertex represent thermally unstable states (ignition points), whereas points to the right of the vertex represent thermally stable states (operating points). For convenience, the vertex of the above thermal stability curve has been chosen as the target point ('end' point) of our sought-after optimal trajectory. By making this choice, we have picked out – among all possible operating points – the one that is characterized by the lowest plasma energy content. As for the starting point of our system trajectory, clearly we must require that it be representative of a well-formed, post-breakdown plasma. Conventionally, in our simulations, we have taken it to be defined by the following plasma conditions: $\tilde{T} = 1$ keV and $\bar{n} = 10^{20}$ m^{-3}.

The *ignition brachystochrone* (i.e. the goal of the calculations performed in this paper) is shown in Fig. 1 as a solid curve connecting the assigned starting and end points. As was anticipated in Sec. 3, it is constructed out of three smooth

† Albeit often in a slightly different form, known as *Coppi's ubiquitous mode scaling*.

‡ That the fastest path to ignition should go through the lowest point of the Cordey pass (i.e. the saddle point of the function F) is clearly something that fits in with our physical intuition.

https://doi.org/10.1017/S0022377801008911 Published online by Cambridge University Press

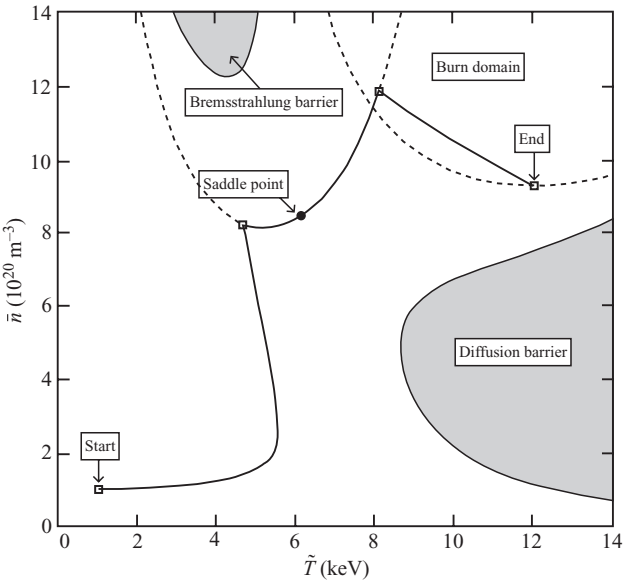

Figure 1. Ignition brachystochrone for the OMITRON device on the basis of *Lackner–Gottardi scaling*. The evolution time from start to end is 4.95 s.

sections joining at corner points: the three sections (ordered from the starting point to the end point) are solutions of (16), (17), and (18), respectively. The way in which the brachystochrone unfolds – that is, the way the brachystochrone kernel curve is first approached and then left – seems to comply with the guiding rule that one must stay on the brachystochrone kernel curve for as long as possible. On more specific grounds, the first rapid rise in density at relatively low temperature is justified by the advantage of storing energy with great efficiency at an early time in the plasma, by exploiting strong low-temperature Ohmic heating. The second density rise (which takes place after the crossing of the Cordey-pass saddle point) is once again justified by the advantage of steering into a region of favourable energy balance (brought about in this case by the prominence of α-particle heating).

The transit time calculated for the *ignition brachystochrone* is, by definition, the shortest possible among the transit times of all possible alternative trajectories.† For the case depicted in Fig. 1, the brachystochrone transit time is found to be 4.95 s. In order to judge whether or not this is 'fast enough', we must compare it with an 'effective' (i.e. constant-current equivalent) pulse duration calculated for the OMITRON device, to which our simulation refers. In the OMITRON development work, this 'effective' pulse duration, from engineering considerations, was assessed to be 6.5 s (Sestero 1997). For the example illustrated in Fig. 1, therefore, there appear to exist a comfortable time

† Direct comparisons with transit times calculated for a number of alternative trajectories – arbitrarily drawn to connect the assigned starting and end points under the assumed constraints – have practically confirmed this result. Such verifications have concurrently produced an *empirical* check of the fact that the existence of the minimum transit time – established by the variational procedure only *in the small* – is a result that also holds *in the large* (i.e. in an absolute sense). A rigorous mathematical proof thereof has not been attempted here, however.

https://doi.org/10.1017/S0022377801008911 Published online by Cambridge University Press

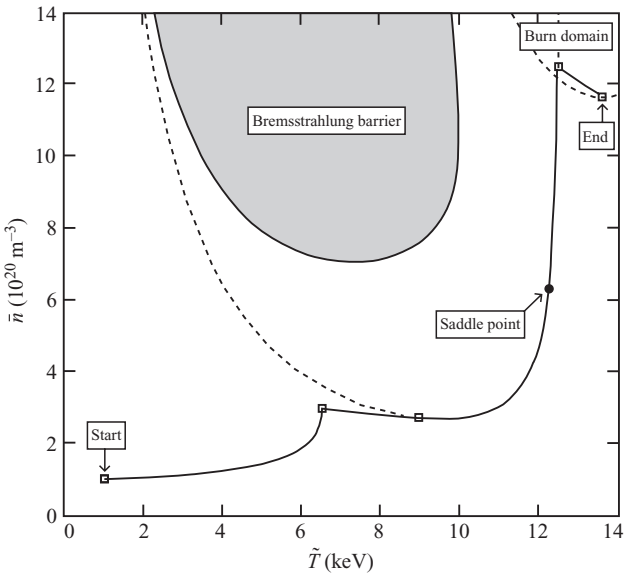

Figure 2. Ignition brachystochrone for the OMITRON device on the basis of *ITER-P89 scaling*. The evolution time from start to end is 7.87 s.

margin for the plasma system to reach the targeted operating point during the available pulse duration.

So much for our first example. It is interesting to see, for comparison, what can happen in other circumstances too. In Fig. 2, a different case is illustrated, in which the Lackner–Gottardi scaling for the energy confinement time has been replaced by the equally well-known *ITER-P89 scaling* (everything else in the simulation being left unchanged). It turns out that this scaling is somewhat less favourable than the Lackner–Gottardi scaling: indeed, the brachystochrone transit time for this case is found to be 7.87 s. This value, in the context of concern here (referring again to the above quoted time limit of 6.5 s), is actually somewhat too long.

However, in the example of Fig. 2, there is another feature worth calling attention to. Indeed, this is one of those cases (anticipated in Sec. 3) in which the very construction of the brachystochrone is different from the standard recipe that is illustrated in Fig. 1. From start to end, in fact, there are four pieces to the brachystochrone (instead of three), these four pieces being solutions of (16), (18), (17), and (18) again, respectively. The additional piece is actually the second, defined as the particular solution of (18) that is tangent to the brachystochrone kernel curve. The reason for such a four-piece construction is that a three-piece construction of the type exploited in Fig. 1 would have led to a *violation of the constraint on the rate of density decrease* (just to the right of the first corner point, in fact). We must, in any case, be aware that other types of brachystochrone construction may be met, in principle, when tinkering with simulation parameter values, the examples depicted in Figs 1 and 2 being just two out of a set of possible circumstances.

https://doi.org/10.1017/S0022377801008911 Published online by Cambridge University Press

6. Concluding remarks

Within the framework of the simplified plasma simulation model dealt with in this paper, it has been made clear that the goal of pursuing the optimum trajectory toward the chosen burning regime is reduced to the issue of implementing an appropriate density control scheme during the heating-up phase of the plasma. Physical and technological limits on the achievable density rates of change have been taken into account in a fundamental way, through the specification of (14) or, equivalently, (15). The form of the latter relations has been taken to be very simple, as appropriate to a pilot calculation, but no problem of principle forbids changing them to more realistic expressions, as may be suggested in the future by actual operation experience with specific devices.

To be sure, in the idealized mathematical treatment of the presented optimization procedure, *corner points* occur at certain positions along the ignition brachystochrone (as previously noted and discussed). At such corner points, the regime of density control must, in principle, change abruptly. This is, of course, impossible to achieve in practice: any realistic density control scheme would indeed result in the corners of the brachystochrone being more or less significantly rounded off. However, the increase in system transit time resulting from this is expected not to be of particular importance.

In spite of all the positive features noted above, it must be realized that the time is not yet ripe for introducing the optimization machinery developed above into the design guidelines for currently investigated non-superconducting ignition experiments. The blame for this is indeed to be laid on the circumstance that the (theoretical or empirical) scaling laws that we are currently using are still quite dubious and deceptive: they are much too ambiguous, indeed, even to allow a plausible assessment of the overall ignition capability of currently proposed ignition devices – let alone to allow a meaningful spelling out of the peculiarities of ignition-path optimization. It is thus expected that the procedure illustrated in this paper will yield important practical results chiefly at some future time, when we shall know more about energy confinement in burning (or nearly burning) plasmas.

On the above grounds, we must issue a warning against considering the results of the previous sections a trustworthy prediction of plasma performance in the OMITRON proposed experiment. In this respect, indeed, in addition to the above uncertainties regarding the employed scaling laws, we must consider the circumstance that in our simulation, for the sake of simplicity, we have made a number of conservative modelling choices – the most important of which is that of limiting ourselves to a global, zero-dimensional description of plasma behaviour. It is well known, in fact, that this type of plasma modelling (because of the rigidity introduced in the radial profiles of the various physical quantities involved) unavoidably yields partially unfaithful results (leaning, in fact, somewhat to the pessimistic side). With respect to this, it is obvious that the extension of the procedure outlined in this paper to one-dimensional plasma simulation models (that is, models constructed in terms of energy transport coefficients rather than of global energy confinement times) would be a highly desirable development: but we must realize that it is not going to be an easy task to accomplish.

References

Barberis, U., Lanzavecchia, L., Palmieri, R., Pirozzi, M., Pizzuto, A. and Sestero, A. 1993 In: *Fusion Technology 1992*, *Proceedings of XVII SOFT* (ed. C. Ferro, M. Gasparotto and H. Knoepfel), p. 1616. North-Holland, Amsterdam.

Elsgolc, L. E. 1962 *Calculus of Variations*, pp. 31–33. Pergamon Press, London.

Garfinkel, B. 1967 Inequalities in a variational problem, Part B. In: *Topics in Optimization* (ed. G. Leitmann). Academic Press, New York.

Sestero, A. 1997 Technical Report ENEA-RT/ERG/FUS/97/17.